Int. J. Solids Structures Vol. 27, No. 7, pp. 833–847, 1991
Printed in Great Britain.

0020–7683/91 $3.00+.00

EFFECTS OF A FRICTIONAL INTERFACE ON THE LOAD DIFFUSION FROM A BROKEN FILAMENT EMBEDDED IN AN ELASTIC MEDIUM

BULENT AKSEL and CHUNG-YUEN HUI
Theoretical and Applied Mechanics Department, Cornell University, Ithaca, NY 14853, U.S.A.

and

DIMITRIS C. LAGOUDAS
Department of Civil Engineering, Rensselaer Polytechnic Institute, Troy, NY 12180, U.S.A.

(*Received* 8 *August* 1989; *in revised form* 28 *February* 1990)

Abstract—The effects of a frictional interface on the load diffusion from a broken fiber to the surrounding matrix material and the extent of debonding near the fiber break in a single-fiber reinforced composite of infinite extent are studied by using the finite element method. The numerically computed axial load carried by the fiber for the perfectly bonded case is first compared with analytical results. Then, the normal and shear stresses on the interface, the extent of the slip zone and the axial load of the fiber are evaluated for different frictional coefficients and material parameters for both the fiber and the matrix. A shear-lag analysis is also carried out to obtain a closed form approximate solution of the fiber load diffusion problem. The extent of the slip zone and the stresses predicted by the shear-lag model are compared with the finite element method results.

1. INTRODUCTION

The problem of load diffusion from a broken fiber into its surrounding matrix has been considered by many authors in various degrees of sophistication. Starting with a simple shear-lag analysis in the work of Cox (1952), more elaborate analyses have appeared over the years with a recent attempt by Whitney and Drzal (1987) that uses approximate stress fields only close to the fiber break. Muki and Sternberg (1971) solve the load diffusion problem as an exact 3-D elasticity problem for the surrounding matrix but they consider the fiber to have a rod-like behavior. The exact solution to the load diffusion problem when both the fiber and matrix are taken to be isotropic linearly elastic and with perfectly bonded interface is given by Ford (1973). Due to the difference in the stress singularity near the fiber break, Ford's solution in the crack tip region significantly differs from that of Muki and Sternberg.

Experimental evidence (i.e. Netravali *et al.*, 1987, 1990) points out that for a wide range of material parameters, the high stresses near the crack tip are relaxed by the failure of the interface, leading to interface crack growth. The growth of interface cracks contributes significantly to the fracture toughness of the composite. On the negative side, interface failure is the principle cause of stiffness reduction in composites. To quantify this phenomenon, one must deviate from the assumption of a perfectly bonded interface adopted in the work of Muki, Sternberg and Ford mentioned above, and explicitly include the interface constitutive description in the stress analysis. Such an analysis was carried out by Dollar and Steif (1988), who investigated the problem of interface failure near a fiber break using a Coulomb frictional interface model. To simplify their analysis, they solve a two-dimensional plane strain contact problem where both the matrix and the fiber have the same material properties. In this work we will remove these restrictions and consider the axisymmetric problem of a broken fiber embedded in an infinite matrix under the action of transverse normal pressure with a uniform axial strain applied far away from the fiber break. There are no restrictions placed on the material properties of the fiber and the matrix, which for the purposes of this work will be assumed to be linearly elastic and isotropic. Instead of using the integral equation formulation as in Dollar and Steif, the above stated

problem is analyzed by using the finite element method. An analytic result, based on the shear-lag model (Piggott, 1980; Budiansky *et al.*, 1986) is then developed to gain insight on how the various material parameters affect the deformation and stress fields (in the average sense) near the fiber break. These analytic results are then compared with the numerical results obtained by the finite element method.

The constitutive behavior of interfaces depends on factors such as material processing during manufacturing and the mechanical and chemical compatibility of matrix and fiber phases of the composite system. Reedy (1985) proposed several models to describe the constitutive behavior of the fiber–matrix interface. These models describe linearly elastic, elastic–perfectly plastic and frictional interfaces. His analysis is only approximate since a shear-lag model is used. Because of its significance in the debonding process in many composite systems and also to make contact with the work of Dollar and Steif, a frictional interface model will be used in this study.

When studying the underlying processes of failure in fiber reinforced composites, it is often necessary to consider the interaction of broken fibers with their neighbors. Typically, a broken fiber will induce a stress concentration on adjacent fibers and the magnitude and extent of such stress concentrations are of considerable interest, e.g. in the statistical analysis of composite tensile strength. These interaction effects are not addressed in this work. Our aim is to focus attention on the influence of the frictional interface on load diffusion. However, the results presented in this work can also be applied directly to experiments involving micro composites which are well approximated by the geometry of our analysis (Netravali *et al.*, 1987, 1990).

2. FORMULATION OF THE PROBLEM

The geometry of the problem to be studied is shown in Fig. 1. The broken fiber is a circular cylinder of radius a and is assumed to be isotropic linearly elastic with Young's modulus E_f and Poisson's ratio ν_f. The z-axis of the cylindrical coordinate system (r, θ, z) coincides with the symmetry axis of the fiber with the origin located at the center of the circular crack, which lies on the plane $z = 0$. The infinite matrix surrounding the fiber is also assumed to be linearly elastic with Young's modulus E_m and Poisson ratio ν_m.

As in Dollar and Steif (1988), the fiber is free to slide along the interface $r = a$ were it not for an applied pressure at infinity, i.e. $\sigma_{rr}^m(r \to \infty, z) = -p$ where $p > 0$ and the superscript m refers to matrix. After the application of the compressive stress $-p$, an uniaxial strain $\varepsilon_{zz} = \varepsilon_\infty$ is applied monotonically at $z \to \infty$ to both the fiber and the matrix.

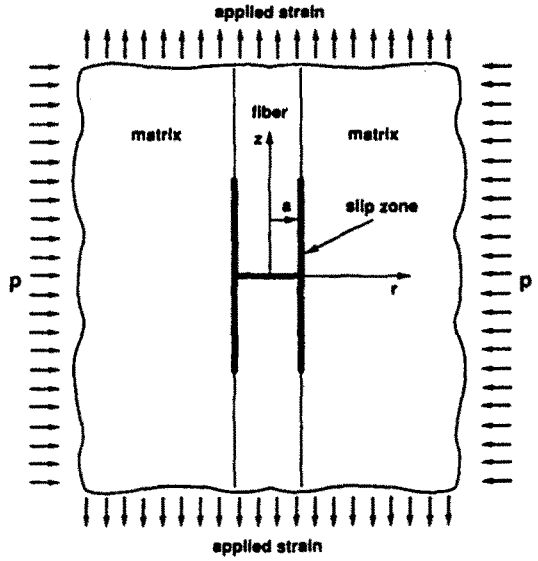

Fig. 1. Problem definition—single fiber in an infinitely extended matrix.

Continuity of tractions is enforced on the fiber–matrix interface at $r = a$. However, displacement discontinuity is allowed to exist according to the Coulomb frictional model. Following Dollar and Steif, at any given instant in the loading history,

$$|\sigma_{rz}| < \mu|\sigma_{rr}|, \quad \sigma_{rr} < 0, \quad \Delta u_z = 0,$$
$$|\sigma_{rz}| = \mu|\sigma_{rr}|, \quad \sigma_{rr} < 0, \quad \operatorname{sgn}\left(\frac{\mathrm{d}(\Delta u_z)}{\mathrm{d}t}\right) = \operatorname{sgn}(\sigma_{rz}), \tag{1}$$

where $\Delta u_z \equiv \lim_{\varepsilon \to 0} [u_z^m(a+\varepsilon, z) - u_z^f(a-\varepsilon, z)]$. The above expresses the stick–slip condition, while the open condition (separation of the fiber and matrix phases) is defined by $\sigma_{rr} = \sigma_{rz} = 0$, $\Delta u_r > 0$ at the interface, where $\Delta u_r \equiv \lim_{\varepsilon \to 0} [u_r^m(a+\varepsilon, z) - u_r^f(a-\varepsilon, z)]$. $u_r(r, z)$ and $u_z(r, z)$ denote the radial and the axial displacements and the superscripts f and m refer to the fiber and matrix respectively. Mu (μ) is the coefficient of friction. Note that $u_\theta \equiv 0$ because of the axial symmetry in the geometry, material properties and loading.

3. NUMERICAL SCHEME

The following normalized variables are introduced to expedite the analysis:

$$\hat{r} = r/a, \quad \hat{z} = z/a,$$
$$\hat{u}_i = u_i/(a\varepsilon_\infty), \quad \hat{\sigma}_{ij} = \sigma_{ij}/p, \tag{2}$$

where a "$\hat{}$" denotes a normalized quantity. From dimensional considerations, the normalized $\hat{u}_i$ and $\hat{\sigma}_{ij}$ depend only on $\hat{r}$, $\hat{z}$, μ, ν_f, ν_m, $\lambda = E_m\varepsilon_\infty/p$ and $\beta = E_f/E_m$. In particular, the size of the slip zone l_s depends only on

$$l_s/a = \varphi[\lambda, \beta, \nu_f, \nu_m, \mu], \tag{3}$$

where φ is an unknown dimensionless function that must be determined from the finite element analysis. The above normalization shows that the effect of increasing the far field axial strain is equivalent to decreasing the confining pressure under the same loading history.

Due to axisymmetry, the solution of the problem is a function of r and z. Symmetry in the geometry and boundary conditions allows us to analyze only one quadrant with the appropriate boundary conditions. Axisymmetric Q8 elements (quadratic interpolation in both directions) are used throughout the analysis. Although it is impossible to duplicate the singular behavior in the stress fields of a crack ending on a bimaterial interface by using quadratic interpolations, we found, by careful selection of element sizes, that it is possible to localize inaccuracies to a very small region compared with a. For this reason the smallest element at $\hat{r} = 1$, $\hat{z} = 0$ on both fiber and matrix sides is chosen to be a square of size $0.006a$. The element size in the matrix increases geometrically by a constant factor of 1.65 in the r direction, whereas the element size in the fiber increases geometrically by a constant factor of 1.43 in the negative r direction. The element size in the z direction increases geometrically by a constant factor of 1.55 for both the fiber and matrix. As a result of the geometric increase of the element size in both r and z directions, a fine mesh near the fiber break and the interface is generated. The outer limits of the region to be analyzed are chosen as $\hat{r}_\infty = 25$, $\hat{z}_\infty = 25$ (in some cases $\hat{z}_\infty$ has been extended to 100). The choice of these finite length dimensions to simulate infinity has been verified by examining the far field stress state after the analysis. To summarize: there are 12 elements in the fiber in the r direction and 20 elements in the z direction. In the matrix, there are 18 elements in the r direction and 20 elements in the z direction. Finally, there are 20 interface elements at the fiber–

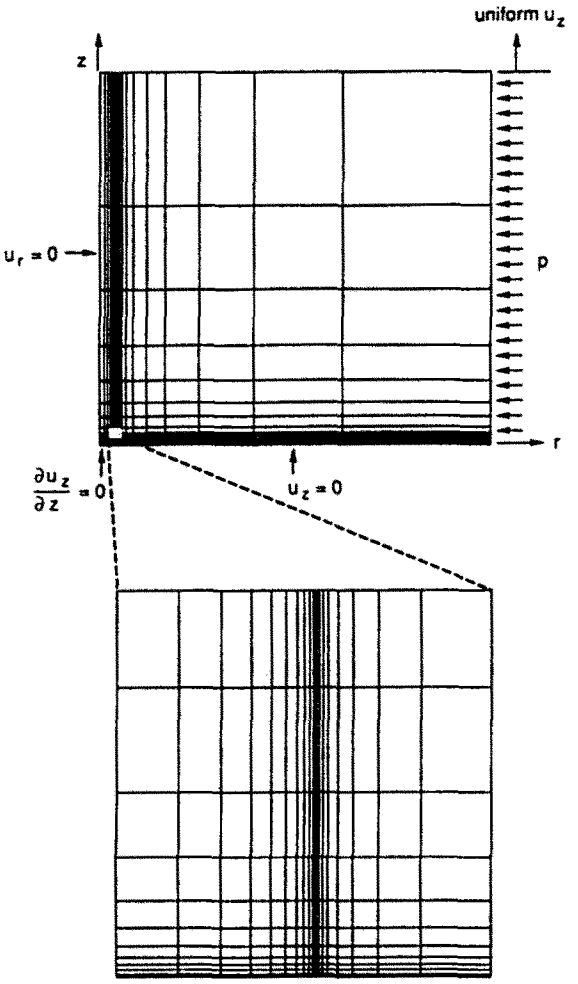

Fig. 2. Finite element mesh and boundary conditions applied for the numerical computations.

matrix interface. In total, the program consists of 620 elements, 1983 nodes and 3966 degrees of freedom (Fig. 2).

Interface elements, based on Coulomb friction with stiff elastic response before sliding, are used for representing the interface between the fiber and the matrix. A frictional interface element is a 1-D element composed of two sides, each having three nodes. An initial distance, which is zero in this case, between the two sides of the element, and a coefficient of friction need to be defined. If the normal component of stress (σ_{rr}) acting on the sides of the element is tensile, the two sides separate and no traction (no normal stress, as well as no shear stress) is carried by the element. If the normal component of stress acting on the sides of the element is compressive, the program checks whether the shear stress applied is higher than the shear limit, that is normal stress applied at that specific point times the coefficient of friction. If the shear stress is higher than the shear limit, the shear stress transferred by the element is taken to be equal to the shear limit. If it is less than the shear limit, the element transfers the shear stress.

Since the solution depends on the loading history, we specify next the load application. In the first step the transverse compressive load p is applied, while at the boundary $\hat{z} \to \infty$ the total axial load is zero (generalized plane strain). Due to the unconstrained deformation in the axial direction, the fiber is under axial tension and the matrix is under axial compression (for a stiff fiber) after the application of the transverse compression. This load alone may result in some initial debonding as soon as the lateral compression is applied. In the second step axial displacement is incrementally applied, which means that the loading parameter λ is increased from the initial value it acquires at the end of the application of the pressure p to its final value.

Another possible way of applying the boundary conditions would be to fix the displacements at $\bar{z} \to \infty$ (plane strain) and, after the lateral compression is applied, to start increasing λ from zero. There is no initial debonding in this case because both the fiber and matrix are initially under compression, but as λ increases the fiber eventually develops axial tension and starts debonding along the interface. It has been found by studying various cases numerically that the two ways of applying the first step of the loading (generalized plane strain vs plane strain) lead to approximately the same solution if the final value of λ is larger than the generalized plane strain λ. Consequently, if experimental results are to be compared with the numerical solutions, it will make practically no difference if the lateral pressure is applied first and then the specimen is constrained to the grips for the axial load, or if the specimen is connected to the grips first and then p is applied, as long as the final λ is sufficiently large.

ABAQUS commercial finite element code is chosen as the analysis tool.

4. RESULTS AND DISCUSSION

To test our numerical scheme, the perfect bond case between the fiber and the matrix is first analyzed. The total axial force acting on the fiber cross-section at certain axial positions is compared with the analytical results reported by Ford (1973). The results are plotted in Fig. 3 for the case of $\beta = 1$ and $\beta = 5$. $P(z)$ is the total axial force applied on the fiber at point z and P_∞ is the total axial force on the fiber at infinity. The close correlation between the two results justifies the selection of the finite element mesh.

After reproducing the solution of the perfect bond case, the program is modified to include the frictional interface. A perfectly bonded interface predicts that both the shear and normal stresses have singularities at the fiber break, which leads to the development of the slip zone and the possibility of separation between the fiber and the matrix. Our finite element analysis showed that, for values of the frictional coefficient μ between zero and one, no separation takes place when the elastic modulus of the fiber E_f is greater than or equal to the elastic modulus of the matrix E_m. This conclusion is in agreement with the asymptotic results reported in Cook, and Erdogan (1972). It is also found that for $0 < \mu < 1$ and if no external pressure is applied, i.e. $p = 0$, slip occurs throughout the total length of the interface even for very small applied axial tension. This means that the normal stresses generated by the uniaxial tension are not sufficient enough to give rise to a shear limit that will withstand the shearing stresses generated by the same loading. Therefore, fiber pullout takes place. This result should not come as a surprise, because experimental evidence supports that there is a bond strength between the fiber and the matrix (Netravali *et al.*, 1987). Friction takes over after the bond is broken. In many cases also the manufacturing process introduces residual stresses. To simulate this behavior, an additional pressure p is applied at $r \to \infty$, before the axial loading is applied.

Figures 4, 5, 6 and 7 show selected numerical results for the shear and normal stresses along the interface and the axial load carried by the fiber as a function of the distance away

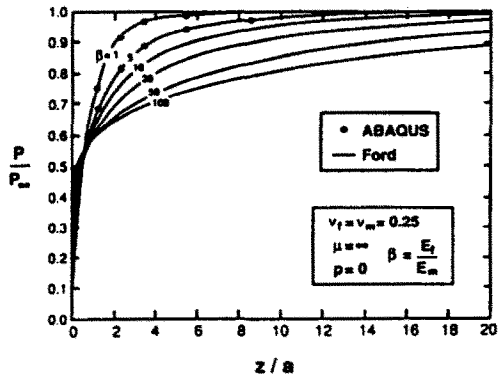

Fig. 3. Comparison of the numerical results for the perfect bonding case with the analytical results reported by Ford (1973).

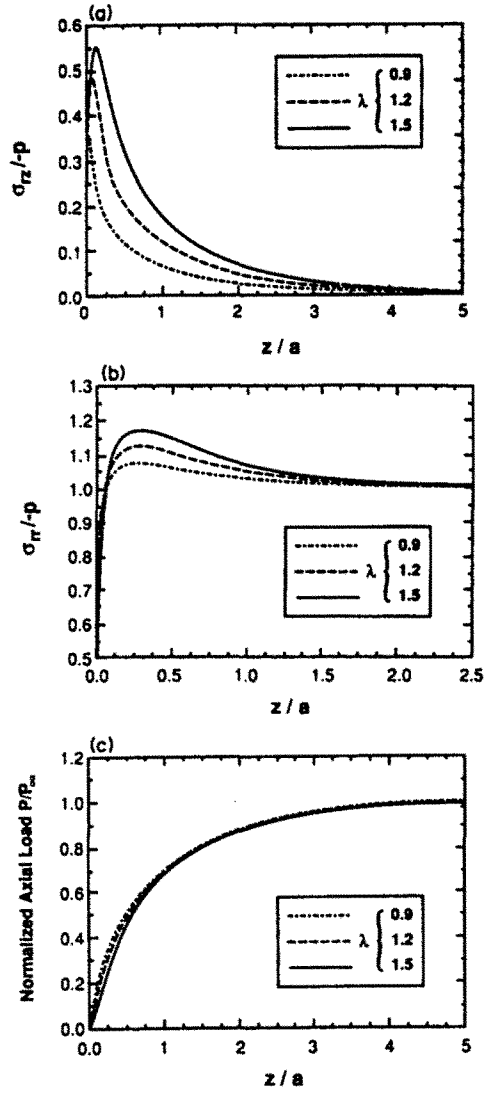

Fig. 4. Interface shear stress, interface normal stress and normalized axial load versus axial distance for various values of $\lambda = E_m\varepsilon_\infty/p$ and for $\beta = E_f/E_m = 1$, $\mu = 0.5$, $\nu_f = \nu_m = 0.25$.

from the fiber break. From the many different cases that have been tested, we present selected results that correspond to a fixed Poisson's ratio for both the fiber and matrix $\nu_f = \nu_m = 0.25$, while the remaining three independent dimensionless material parameters μ, λ and β are varied.

Figures 4a, 4b and 4c show the results for $\beta = 1$ and for a relatively strong interface (frictional coefficient $\mu = 0.5$), for different values of λ. Notice that the absolute value of the shear stress starts from zero and reaches a finite maximum before it decays to zero as $z \to \infty$. The relaxation of the constraint of perfect bonding leads to finite stresses near the crack tip in contrast to the singular stress fields predicted by Ford (1973) for the case of perfect bonding ($\mu \to \infty$). The slip zone extends initially a small fraction of the fiber radius and increases with increasing λ. The normal stress behaves similarly, but it decays to a finite value given by the formula

$$\bar{\sigma}_{rr}^f = \frac{\sigma_{rr}^f}{p} = -\frac{2(1-\nu_m^2)-(\nu_f-\nu_m)\lambda}{(1+\nu_m)+(1+\nu_f)(1-2\nu_f)/\beta}. \tag{4}$$

The above formula is exact and is obtained from solving the problem of a single unbroken fiber imbedded in an infinitely extended matrix and subjected to the same loading conditions, that is ε_∞ applied in the axial direction and pressure p applied in the transverse direction.

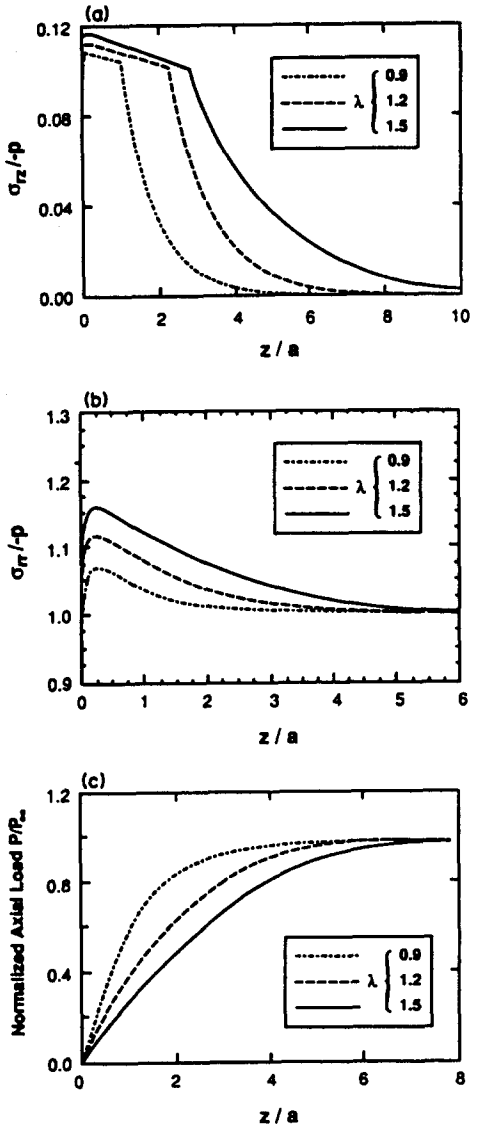

Fig. 5. Interface shear stress, interface normal stress and normalized axial load versus axial distance for various values of $\lambda = E_m\varepsilon_\infty/p$ and for $\beta = E_f/E_m = 1$, $\mu = 0.1$, $\nu_f = \nu_m = 0.25$.

For the values of λ used, which result in a sufficiently small slip zone, the axial load recovery occurs in about three fiber radii. We mention that the same normal stress on the interface can be generated by cooling the infinite composite cylinder an amount given by

$$\Delta T = \frac{-2p(1-\nu_m^2)}{E_m[\alpha_m(1+\nu_m)-\alpha_f(1+\nu_f)]},$$

where α_f, α_m are the (isotropic) thermal expansion coefficients of fiber and matrix, respectively. The above formula has been obtained by assuming ε_∞ to be the same in both the mechanical and thermal problems and by requiring σ_{rr}^f to be the same on the interface for both problems. It can be used to connect a given ΔT to its equivalent mechanical load p.

Figures 5a, 5b and 5c are similar to those discussed above but for a relatively weak interface ($\mu = 0.1$). The basic difference in the results from the previous case is the increase in the slip zone and the almost constant shear stress along the interface for the extent of the slip zone. Small increases in the applied strain now cause larger increases in the slip zone. Notice that the axial load in the broken fiber recovers initially almost linearly, as a result of a constant shear stress along the interface in the slip zone.

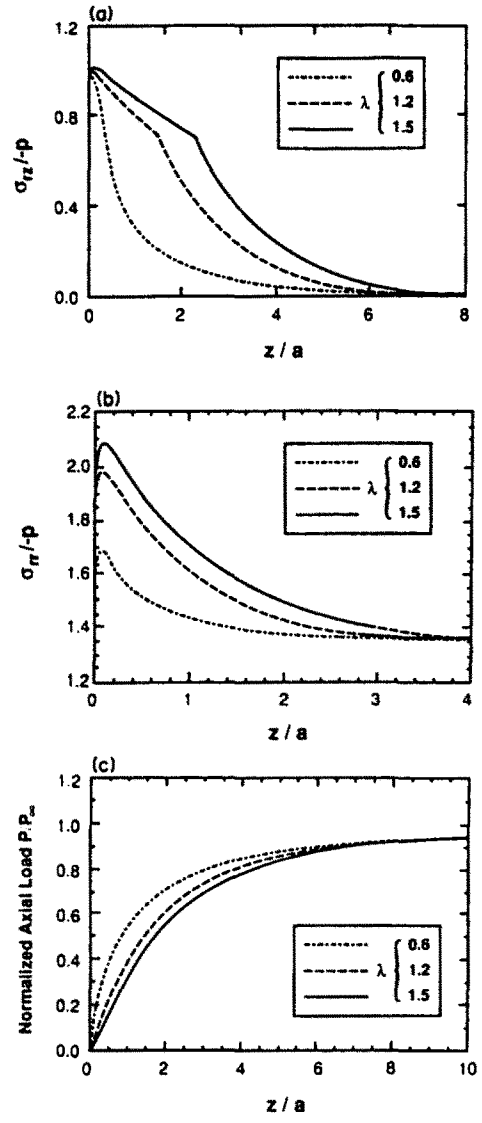

Fig. 6. Interface shear stress, interface normal stress and normalized axial load versus axial distance for various values of $\lambda = E_m\varepsilon_\infty/p$ and for $\beta = E_f/E_m = 5$, $\mu = 0.5$, $\nu_f = \nu_m = 0.25$.

Figures 6 and 7 examine the shear and the normal stresses along the interface and the axial load in the fiber for the case of two dissimilar materials. The case of $\beta = 5$, which is typical for ceramic matrix fibrous composites, is presented, where it becomes clear that a stiffer fiber causes a larger slip zone for the same values of the frictional coefficient μ and the loading parameter λ than in the case of $\beta = 1$.

The normal component of stress σ_{zz}^m ahead of the fiber break ($z = 0$) along the radial direction is plotted in Fig. 8 for the case $\beta = 5$ and for different values of λ. Even though there is a stress concentration close to the crack tip, the stress singularity is relaxed by the loss of constraint due to the interface slip, thus preventing a crack growth in the radial direction.

In Figs 9 and 10 the shear and normal stresses along the interface and the axial load in the fiber are presented for a typical glass epoxy fibrous composite with $\beta = 25$ and frictional coefficients $\mu = 0.5$ and $\mu = 0.3$ for various values of the loading λ. Notice that for about the same values of slip length with the previous cases, the amount of loading is substantially smaller due to the high stiffness ratio β. The frictional coefficient must also be greater than 0.3 to prevent extensive interface slip (greater than 25 fiber diameters) for small values of λ. To enforce small λ, the lateral pressure p is applied under plane strain conditions, in which case λ starts increasing from zero. Finally, in Fig. 11 the slip zone

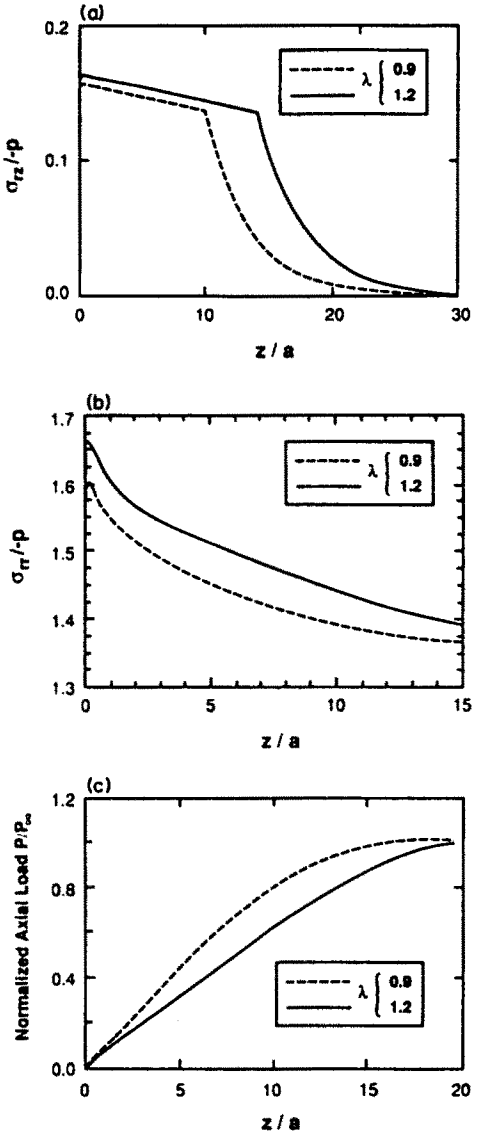

Fig. 7. Interface shear stress, interface normal stress and normalized axial load versus axial distance for various values of $\lambda = E_m\varepsilon_z/p$ and for $\beta = E_f/E_m = 5$, $\mu = 0.1$, $\nu_f = \nu_m = 0.25$.

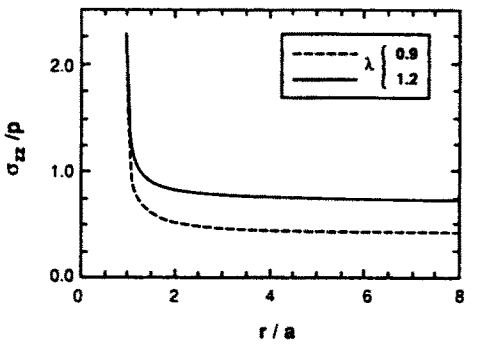

Fig. 8. Normal stress $\bar{\sigma}_{zz}^m$ in the matrix ahead of the fiber break for various values of $\lambda = E_m\varepsilon_\infty/p$ and for $\beta = E_f/E_m = 5$, $\mu = 0.1$, $\nu_f = \nu_m = 0.25$.

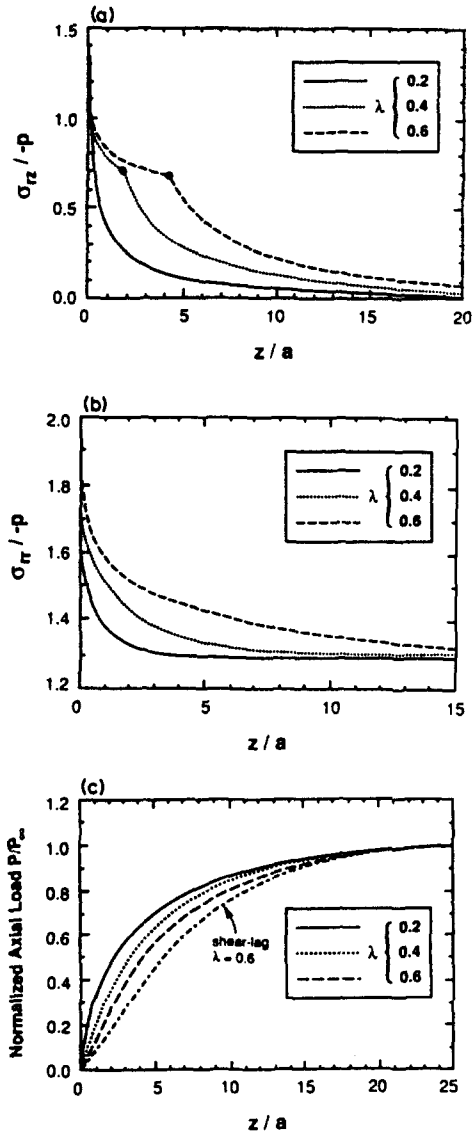

Fig. 9. Interface shear stress, interface normal stress and normalized axial load versus axial distance for various values of $\lambda = E_m \varepsilon_z / p$ and for $\beta = E_f/E_m = 25$, $\mu = 0.5$, $\nu_f = 0.22$, $\nu_m = 0.35$.

length is plotted as a function of the loading λ and parametrized by the frictional coefficient μ.

The above results show that, in the presence of a frictional interface, stress gradients are much smaller than in the perfect bond case. For this reason, an extremely refined mesh is not necessary for reliable results. An important outcome of this study is that the broken fiber carries less load in the region close to the fiber break, with a longer ineffective length as the frictional coefficient decreases. Therefore, neighboring intact fibers will be overstressed over larger lengths than they will be overstressed in the case of perfect bonding. This result is important for the determination of the composite strength based on micro-mechanical models.

5. A SHEAR-LAG MODEL

A shear-lag model is developed in which the axial stress on any cross-section of the fiber is taken to be constant and the reaction to extension and shear in the matrix is decoupled. The infinite matrix surrounding the fiber is replaced by a cylinder of radius R_m that can only carry shear forces. The shear force from the broken fiber is transferred by this cylinder to its outer edge at $r = R_m$, where the resistivity of the matrix to axial stretching

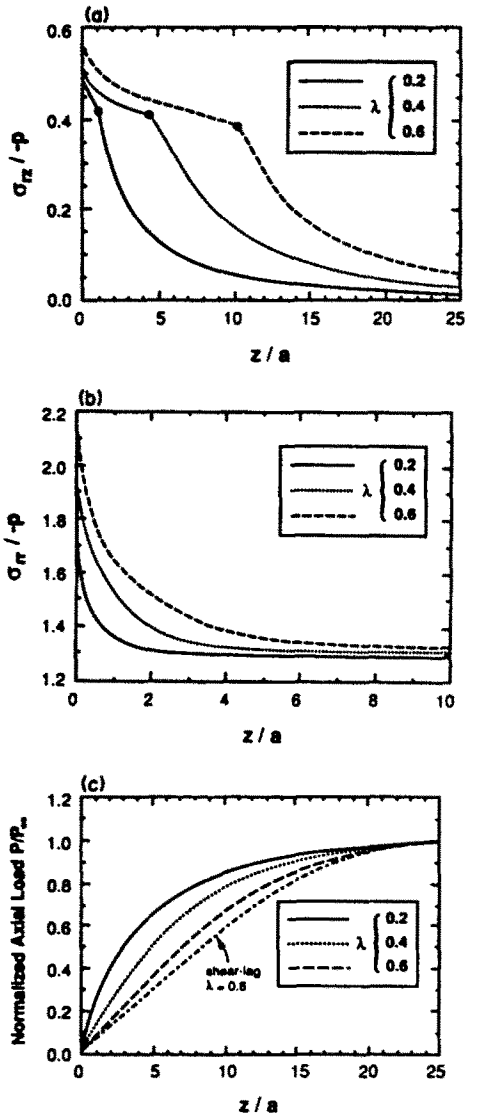

Fig. 10. Interface shear stress, interface normal stress and normalized axial load versus axial distance for various values of $\lambda = E_m\varepsilon_\infty/p$ and for $\beta = E_f/E_m = 25$, $\mu = 0.3$, $\nu_f = 0.22$, $\nu_m = 0.35$.

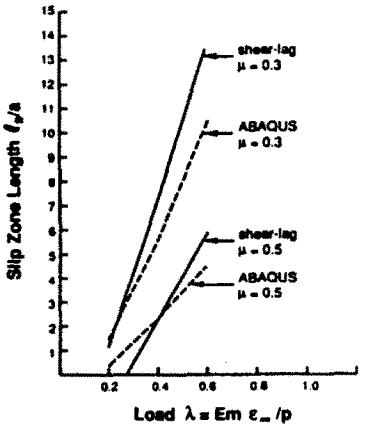

Fig. 11. Interface slip zone length versus loading parametrized by the frictional coefficient for a glass/epoxy fibrous composite ($\beta = E_f/E_m = 25$, $\nu_f = 0.22$, $\nu_m = 0.35$).

is assumed to be concentrated. This simplification is equivalent to considering the fiber and matrix as linear elastic springs connected with shear springs.

In the subsequent equations, the subscript f will refer to quantities characterizing the fiber and the subscript m to quantities characterizing the matrix. There are three equilibrium equations that have to be satisfied. They represent local equilibrium of forces in the fiber (σ_f), the cylindrical portion of the matrix that carries only shear (τ_{rz}) and the outer thin layer of matrix that carries the tensile load (σ_m). These equations are (Budiansky *et al.*, 1986)

$$\frac{d\sigma_f}{dz} + \frac{2}{a}\tau_i = 0, \tag{5}$$

$$\frac{\partial \tau_{rz}}{\partial r} + \frac{\tau_{rz}}{r} = 0, \tag{6}$$

$$\frac{d\sigma_m}{dz} - \frac{2\pi a}{A_m}\tau_i = 0. \tag{7}$$

The global equilibrium of forces takes the form

$$A_f\sigma_f^\infty + A_m\sigma_m^\infty = A_m\sigma_m^0, \tag{8}$$

where $A_f = \pi a^2$ and $A_m = \pi(R_m^2 - a^2)$ are the cross-sectional areas of the fiber and the matrix, respectively. The normal stress in the fiber and the matrix as $z \to \infty$ are given respectively by $\sigma_f^\infty = E_f\varepsilon_\infty$ and $\sigma_m^\infty = E_m\varepsilon_\infty$, while σ_m^0 is the normal stress in the matrix at $z = 0$. The interface shear stress is denoted by τ_i. The ratio $\sigma_m^0/\sigma_m^\infty = c$ gives the average stress concentration in the matrix due to the fiber break and it can be determined from eqn (8) if R_m is known. Since the matrix is infinitely extended, it seems more reasonable to assume the value of c and then calculate R_m from (8). If we make the assumption that $c = 2$, R_m is given by

$$\hat{R}_m = \frac{R_m}{a} = (\beta + 1)^{1/2}. \tag{9}$$

Later, we will see that only ln ($\hat{R}_m$) enters into the calculations, therefore the results of the shear-lag model are not sensitive to the exact selection of R_m.

Assuming that frictional slip occurs, eqns (5), (6) and (7) are solved for the displacements of the fiber and the matrix, first in the slip region, $0 \leqslant z \leqslant l_s$, and then in the bonded region $l_s \leqslant z < \infty$, where l_s is the length of the slip zone. The constitutive equations used for the fiber and the matrix are

$$\sigma_f = E_f\frac{dw_f}{dz}, \quad \tau_{rz} = G_m\frac{\partial w}{\partial r}, \quad \sigma_m = E_m\frac{dw_m}{dz}, \tag{10}$$

where $w_f(z)$, $w(r, z)$ and $w_m(z)$ are the displacements in the z direction of the fiber, the cylindrical portion of the matrix that carries the shear and the outer layer of the matrix that carries the tension, respectively.

The boundary conditions (nondimensionalized form) for the shear-lag analysis are given by

$$\hat{\sigma}_f(0) = 0, \quad \hat{\sigma}_m(0) = \hat{\sigma}_m^0 = 2\lambda, \quad w_m(0) = 0,$$
$$\hat{\sigma}_f(\infty) = \hat{\sigma}_f^\infty = \beta\lambda, \quad \hat{\sigma}_m(\infty) = \hat{\sigma}_m^\infty = \lambda. \tag{11}$$

The interface conditions are:

$$\tau_i(z) = \tau_s, \quad w(R_m, z) = w_m(z), \quad 0 \leqslant z < l_s,$$
$$w_f(z) = w(a, z), \quad w(R_m, z) = w_m(z), \quad l_s \leqslant z < \infty, \tag{12}$$

where $|\tau_s|$ is the strength of the interface in shear (we use the absolute value to indicate that τ_s itself corresponds to the shear stress on the interface in the slip zone and it has a negative value during the pullout of the fiber). We also require that the displacements w_f, w_m and their derivatives be continuous at $z = l_s$ (matching conditions between the perfectly bonded and the debonded regions). The continuity of the shear stress at the end of the slip zone is expressed by the condition $\tau_i(l_s) = \tau_s$, which allows us to solve for l_s. The shear strength $|\tau_s|$ of the interface is considered a known constant that can be determined either from experiments or from analytical calculations. For the case of Coulomb friction the following formula can be used as a rough estimate for the shear strength:

$$\hat{\tau}_s = \frac{\tau_s}{p} = \mu \hat{\sigma}_{rr}^f = -\mu \frac{2(1-\nu_m^2) - (\nu_f - \nu_m)\lambda}{(1+\nu_m) + (1+\nu_f)(1-2\nu_f)/\beta}. \tag{13}$$

The expression for the normal stress on the interface σ_{rr}^f is taken from (4), which corresponds to the solution of the unbroken fiber problem.

After solving the equilibrium equations subject to the above given boundary, interface and matching conditions, the following results are obtained.

The length of the slip zone l_s is found to be

$$\hat{l}_s = \frac{l_s}{a} = -\frac{\beta\lambda}{2\hat{\tau}_s} - \frac{1}{\xi}, \tag{14}$$

while the relative slip between the fiber and the matrix in the debonded region is given by

$$\Delta\hat{w}(\hat{z}) = \frac{\Delta w(\hat{z})}{a\varepsilon_\infty} = \frac{w_f - w(l, \hat{z})}{a\varepsilon_\infty} = 2(\hat{l}_s - \hat{z})\left[\frac{\hat{\tau}_s}{\beta\lambda}(\hat{l}_s + \hat{z}) + 1\right], \quad 0 \leqslant z \leqslant l_s. \tag{15}$$

The shear stress on the interface τ_i and the normal stress in the fiber σ_f (the axial load carried by the fiber is $P = \sigma_f A_f$) are given by:

$$\hat{\tau}_i(\hat{z}) = \frac{\tau_i(\hat{z})}{p} = \hat{\tau}_s, \quad 0 \leqslant \hat{z} < \hat{l}_s, \tag{16a}$$

$$\hat{\tau}_i(\hat{z}) = \hat{\tau}_s \exp[-\xi(\hat{z} - \hat{l}_s)], \quad \hat{l}_s \leqslant \hat{z} < \infty, \tag{16b}$$

$$\hat{\sigma}_f(\hat{z}) = \frac{\sigma_f(\hat{z})}{p} = -2\hat{z}\hat{\tau}_s, \quad 0 \leqslant \hat{z} < \hat{l}_s, \tag{17a}$$

$$\hat{\sigma}_f(\hat{z}) = -(2\hat{l}_s\hat{\tau}_s + \beta\lambda)\exp[-\xi(\hat{z} - \hat{l}_s)] + \beta\lambda, \quad \hat{l}_s \leqslant \hat{z} < \infty. \tag{17b}$$

The dimensionless constants ξ, β and λ appearing in the above formulae have the evaluations

$$\xi = \left[\frac{2}{\beta(1+\nu_m)} \frac{1}{\ln(\hat{R}_m)}\right]^{1/2}, \quad \beta = \frac{E_f}{E_m}, \quad \lambda = \frac{E_m\varepsilon_\infty}{p}. \tag{18}$$

We note that all of the above shear-lag analysis results have been given in terms of the nondimensional parameters β and λ introduced in Section 3. The additional parameter $\hat{\tau}_s = \tau_s/p$, that enters the shear-lag results and corresponds to the strength of the interface, replaces the coefficient of friction μ of the finite element analysis [i.e. see (13)].

It is of interest to compare the predictions of the simple shear-lag analysis results, namely eqns (14), (16) and (17), with the finite element calculations shown in Figs 4, 5, 6,

7, 9 and 10. The extent of the slip zone is found in the plots of the interface shear stress, Figs 4a, 5a, 6a, 7a, 9a and 10a, as the value of z at which the shear stress changes slope. The predictions of the shear-lag model for the slip zone length $\hat{l}_s$ from (14) are 0.735, 5.535, 2.726 and 20.321 for the cases shown in Figs 4a, 5a, 6a and 7a, respectively, and for applied loading $\lambda = 1.2$. For large values of $\hat{l}_s$ the second term in (14) can be neglected and $\hat{l}_s$ becomes proportional to the fiber stress at infinity $\beta\lambda$ and inversely proportional to the interface shear strength $|\hat{\tau}_s|$. This is shown in Fig. 11, where the shear-lag slip-zone length predictions are compared with the numerical results for the glass/epoxy composite. There is an overestimate of the slip-zone length predictions by the shear-lag model and this is due to the underestimate of the shear stress along the interface in the slip zone. If the shear stress $\hat{\tau}_s$ is corrected according to the results of the finite element analysis, then the predictions of $\hat{l}_s$ from the shear-lag model become closer to the finite element calculations.

If we substitute $\nu_f = \nu_m = 0.25$ into (13), we obtain the evaluation $\hat{\tau}_s = -\mu$ for the interface shear stress for the case $\beta = 1$. As can be seen from Fig. 4a ($\mu = 0.5$), the value $-\sigma_{rz} = 0.5$ ($\hat{\sigma}_{rz}$ in the figure corresponds to $\hat{\tau}_s$ in the slip zone according to the shear-lag model) is a good approximation for the shear stress in the slip zone, while from Fig. 5a ($\mu = 0.1$) we observe that the theoretical prediction, that is $-\hat{\sigma}_{rz} = 0.1$, is also a good approximation for the shear stress [a slight underestimate of the shear stress given by (13) occurs in all comparisons because the evaluation of $\hat{\tau}_s$ by (13) is based on a continuous fiber, without taking into account the additional compressive stress due to the fiber break]. Similar observations are valid for the $\beta = 5$ case, where (13) predicts that the shear stress in the slip zone will be $\hat{\tau}_s = -1.364\mu$ or $-\hat{\sigma}_{rz} = 0.682$ for Fig. 6a ($\mu = 0.5$) and $-\hat{\sigma}_{rz} = 0.1364$ for Fig. 7a ($\mu = 0.1$). We notice that for the case with the smaller frictional coefficient and thus larger slip-zone length (Figs 5a and 7a), the shear-lag assumption of constant shear stress in the slip zone is more justifiable. At the end of the slip zone an exponential decay for the shear stress is predicted by the shear-lag model from (16b) and this is the type of behavior predicted by the finite element method as shown in Figs 4a, 5a, 6a, 7a, 9a and 10a.

The final test for the shear-lag model is the comparison of its prediction for the axial load in the fiber with the finite element calculations. The basic characteristic of the shear-lag model is that in the slip zone the axial load varies linearly with the distance, which is equivalent to the assumption that the shear stress is constant in the slip zone. It is evident from Figs 5c and 7c that this assumption is justified again for large slip zones. The value of $\sigma_f/\sigma_f^{\infty}$ (or P/P_∞) at $\hat{z} = \hat{l}_s = 5.535$ is 0.923 from (17) for $\lambda = 1.2$ and the same value almost results from the finite element analysis, as shown in Fig. 5c. For the case of Fig 7c the value of $\sigma_f/\sigma_f^{\infty}$ (or P/P_∞) at $\hat{z} = \hat{l}_s = 20.321$ is 0.924 from (17) for $\lambda = 1.2$ and it is again very close to the finite element method result, as indicated in Fig. 7c. For the glass/epoxy composite the comparison between the shear-lag results and the numerical results is shown in Figs 9c and 10c.

In summary, the shear-lag analysis predicts accurately the interface shear stress and the axial load in the fiber for small frictional coefficients or large applied strains that lead to relatively large slip-zone lengths ($\hat{l}_s > 5$).

Acknowledgements—This research was conducted using the Cornell National Supercomputer Facility. Partial support by the U.S. Army Research Office through the Mathematical Sciences Institute of Cornell University and the ONR-DARPA/HiTASC program at Rensselaer Polytechnic Institute contract No. N00014-86-K0700 is gratefully acknowledged. The authors also wish to acknowledge the useful remarks and suggestions by the reviewers.

REFERENCES

Budiansky, B., Hutchinson, J. W. and Evans, A. G. (1986). Matrix fracture in fiber-reinforced ceramics. *J. Mech. Phys. Solids* **34**, 167–189.

Cook, T. S. and Erdogan, F. (1972). Stresses in bonded materials with a crack perpendicular to the interface. *Int. J. Engng Sci.* **10**, 677–697.

Cox, H. L. (1952). The elasticity and strength of paper and other fibrous materials. *British J. Applied Phys.* **3**, 72–79.

Dollar, A. and Steif, P. S. (1988). A tension crack impinging upon frictional interfaces, Report SM 88-1, Carnegie-Mellon University.

Ford, E. F. (1973). Stress analysis of a broken fiber imbedded in an elastic medium, Technical Report No. 1, NSF Grant GH-33576, Division of Applied Sciences, Harvard University.

Muki, R. and Sternberg, E. (1971). Load-absorption by a discontinuous filament in a fiber-reinforced composite. *Z. Angew. Math. Phys.* **22**, 809–824.

Netravali, A. N., Henstenburg, R. B., Phoenix, S. L. and Scwartz, P. (1990). Interfacial shear strength studies using the single-filament-composite Test. I: Experiments on graphite fibers in epoxy. *Polymer Composites* (in press).

Netravali, A. N., Stone, D., Ruoff, S. and Topoleski, L. T. (1987). Continuous microindenter pushthrough technique for measuring interfacial shear strength in fiber composites. MSC Report No. 6336, Cornell University.

Piggott, M. R. (1980). *Load-Bearing Fibre Composites*. Pergamon Press, Oxford.

Reedy, E. D., Jr (1985). Fiber stress concentrations in kevlar/epoxy monolayers. *J. Comp. Mater.* **19**, 533–543.

Whitney, J. M. and Drzal, L. T. (1987) Axisymmetric stress distribution around an isolated fiber fragment. *Toughened Composites*, **ASTM STP 937**, (Edited by N. J. Johnston), pp. 179–196. American Society for Testing and Materials, PA.